

Adaptive Convolutional Neural Network for Image Super-resolution

Ziang Wu, Jinwei Xie, Xuanyu Zhang, Tao Wang, Yongjun Zhang, Qi Zhu, Chunwei Tian

Abstract—Convolutional neural networks can automatically learn features via deep network architectures and given input samples. However, the robustness of obtained models may face challenges in varying scenes. Bigger differences in network architecture are beneficial to extract more diversified structural information to strengthen the robustness of an obtained super-resolution model. In this paper, we proposed a adaptive convolutional neural network for image super-resolution (ADSRNet). To capture more information, ADSRNet is implemented by a heterogeneous parallel network. The upper network can enhance relation of context information, salient information relation of a kernel mapping and relations of shallow and deep layers to improve performance of image super-resolution. That can strengthen adaptability of an obtained super-resolution model for different scenes. The lower network utilizes a symmetric architecture to enhance relations of different layers to mine more structural information, which is complementary with a upper network for image super-resolution. The relevant experimental results show that the proposed ADSRNet is effective to deal with image resolving. Codes are obtained at <https://github.com/helloxiaoqian/ADSRNet>.

Index Terms—Dynamic convolutions, dilated convolutions, heterogeneous networks, image super-resolution.

I. INTRODUCTION

Single image super-resolution (SISR) techniques can obtain high-quality images from given low-resolution images (LR), according to solution of ill-posed inverse problems [1, 2]. In recent years, machine learning techniques have obtained huge achievements in various applications, i.e., disease diagnosis [3], classification [4, 5], object recognition [6], multimodal data fusion [7, 8], Metaverse [9, 10] and SISR [11, 12]. Specifically, deep learning techniques with end-to-end architectures have obtained better visual effect in SISR

This work was supported in part by the Basic and Applied Basic Research Foundation of Guangdong Province under grant 2025A1515011566, in part by Leading Talents in Gusu Innovation and Entrepreneurship under grant ZXL2023170, and in part by the Basic Research Programs of Taicang 2024 under grant TC2024JC32. (Corresponding author: Chunwei Tian (Email:chunweitian@163.com) and Tao Wang (Email:twang@nwpu.edu.cn).)

Authors' Contact Information: Ziang Wu, School of Engineering, The Hong Kong University of Science and Technology, Hong Kong, China, ziang.wu@connect.ust.hk; Jinwei Xie, Macao Polytechnic University, Macao, China, xiejinwei8@gmail.com; Xuanyu Zhang, School of Software, Northwestern Polytechnical University, Xi'an, China, xuanyuzhang@mail.nwpu.edu.cn. Tao Wang, School of Computer Science, Northwestern Polytechnical University, Xi'an, China, twang@nwpu.edu.cn; Yongjun Zhang, College of Computer Science and Technology, Guizhou University, Guiyang, China, zyj6667@126.com; Qi Zhu, School of Artificial Intelligence, Nanjing University of Aeronautics and Astronautics, Nanjing, China, zhuqi@nuaa.edu.cn; Chunwei Tian, Shenzhen Research Institute of Northwestern Polytechnical University, Northwestern Polytechnical University, Shenzhen, China, Yangtze River Delta Research Institute, Northwestern Polytechnical University, Taicang, China, chunweitian@163.com.

[13]. Deep convolutional neural networks (DCNNs) use end-to-end architectures rather than manual setting parameters to obtain strong learning abilities to improve visual effects of SISR [14]. Dong et al. designed 3-layer network through pixel transform to convert a low-resolution (LR) image to a high-resolution (HR) image [15]. Although this method can improve resolution of predicted images, it is limited between network depth and performance in SISR. To address this issue, scholars try to enlarge network depth to pursue improved performance in image super-resolution [16]. Stacking small filters is used to achieve a very deep SR network [16]. Additionally, a residual learning technique (RL) is employed on a deep network layer in a network to make a balance between SR performance and computational costs. A deeply-recursive convolutional network (DRCN) [17] and deep recursive residual network (DRRN) [18] can exploit recursive networks to decrease parameters of training a SR model. To reduce computational complexities, some up-sampling operations, such as transposed convolution [19], deconvolution and sub-pixel convolution [20] are set on a deep network layer to amplify low-frequency information for constructing HR images. For instance, a fast SR convolutional neural network (FSRCNN) [21] directly inputted low-resolution images to a deep CNN to obtain low-frequency features and applies a upsampling operation to transform low-frequency features to high-frequency features and obtain HR images. To further improve SR performance, an enhanced deep SR network as well as EDSR used enhanced residual blocks to extract more structural information for image super-resolution [22]. Also, deleting many unnecessary batch normalization can improve effect of training efficiency a SR model [22]. Although these algorithms are effective for SISR, they did not automatically update parameters, according to different scenes. That may cause poor robustness of obtained SR models for complex scenes. we propose a heterogeneous dynamic network for SISR as well as ADSRNet. ADSRNet uses a heterogeneous parallel network to capture more information to improve performance of image SR in this paper. The upper network uses stacked heterogeneous blocks to extract more contexture information in image SR. Also, each heterogeneous block uses different components to achieve dynamically learning parameters to strengthen robustness of our ADSRNet for SISR, according to different scenes. Also, it can prevent long-term dependency problem. The lower network can use a symmetric architecture to enhance relationships of between different layers to obtain more complementary structural information. Quantitative and qualitative analysis show that the proposed method is a good tool for image super-resolution.

Our main contributions can be summarized as follows.

(1) A heterogeneous parallel network is used to facilitate complementary structural information to improve performance for image super-resolution in terms of contextual, hierarchical and salient information.

(2) Dynamic convolutions are embedded into a convolutional neural network to strengthen robustness of obtained SISR model for complex scenes.

(3) An enhanced residual architecture is designed to address long-term dependency for image super-resolution.

The remaining of this paper is listed. Section II describes related work. Section III illustrates the proposed method. Section IV collects massive comparative experimental results. And Section V summarizes our work.

II. RELATED WORK

A. Deep CNNs for Image Super-resolution

Due to the shooting distance, captured images by cameras are unclear. Also, traditional image super-resolution methods need manual setting parameters and complex optimization parameters. To address this issue, deep learning techniques are extended for SISR [23, 24]. For instance, a deep recursive residual network used local residual connection and unit to improve effects of image super-resolution [18]. Alternatively, Yang et al. used recursive and gate units to transfer information shallow layers to deep layers to address long-term dependency problem [25]. To improve efficiency of image SR, given LR images are directly as an input of a convolutional neural network and high-quality images are constructed via an up-sampling operation in deep layer [21]. For instance, Ahn et al. used group convolutions to implement a cascading residual CNN to extract more robustness low-frequency information and decrease the number of parameters without causing significantly performance loss in SISR [26]. Tian et al. exploited symmetric network architecture to mine more accurate low-frequency information for image super-resolution [27]. Zhang et al. extended the depth of network and fully used hierarchical information to afford more low-frequency information for image SR [28]. According to mentioned methods, we can see that deep CNNs are good tools to obtain clearer images and enhanced CNNs are effective for SISR. Thus, we enhanced a CNN to pursue better visual effects in SISR. Differing from previous research, we choose parallel and serial ways to facilitate heterogeneous information to better represent low-frequency structural information to improve visual effects of SISR.

B. Dynamic convolution

Existing CNNs can share parameters to extract useful features for better represent images. However, they may face challenges from varying input images in complex scenes [29]. To address this issue, dynamic convolutions have been introduced [29]. That is, they can dynamically adjust parameters to adaptively learn models for image applications, according to different inputs. For instance, Wan et al. achieved a graph convolution by arbitrarily structuring non Euclidean data for hyperspectral image classification [30]. Alternatively, Ding et al. can atomically find valuable receptive fields of each target

node to adaptively capture neighbor information in hyperspectral image classification [31]. To deal with native effects from incurring artifacts of textureless and edge regions, Duan et al. can dynamically generate kernels by region context from input images to better achieve image fusion [32]. To adaptively adjust brightness of enhanced images, Dai et al. fused Taylor expansion and dynamic convolution into a Retinex to intelligently improve clarity of low-light images and degree of brightness flexibly [33]. To extract more context information, Hou et al. proposed dynamic hybrid gradient convolution and coordinate sensitive attention to enhance boundary information extraction for remote sensing image segmentation [34]. To find more high-frequency information, Shen et al. used a spatially enhanced kernel generation to dynamic learn high-frequency and multi-scale features to better achieve visual effect in image restoration [35]. Additionally, Tian et al. exploited relations of channels to extract richer low-frequency information for SISR [27]. Based on these examples, dynamic convolutions can dynamically learn parameters to improve robustness of an obtained CNN for SISR, according to different inputs. Thus, we use dynamic convolutions to guide a CNN to update parameters to strengthen adaptability in terms of recovering high-quality images for different scenes. Differing from previous research, a heterogeneous network architecture can facilitate more robustness features to generate high-quality images.

III. PROPOSED METHOD

A. Network Architecture

The proposed 18-layer ADSRNet contains two 16-layer parallel heterogeneous networks and a 2-layer construction block. The 16-layer parallel heterogeneous is composed of a 16-layer heterogeneous upper network and a symmetrical lower network. The heterogeneous upper network is composed of a Conv+ReLU (CRU) and five stacked heterogeneous blocks, which can extract more contexture information for image super-resolution. A CRU is a composite of a convolutional layer and a ReLU operation, which is used to extract non-linear information from given low-resolution images. Also, its input and output channel numbers are 3 and 64, respectively. Its kernel size is 3×3 . These stacked heterogeneous blocks utilize different convolutional layers (i.e., dynamic and common convolutional layers) and ReLU to dynamically adjust parameters to obtain robust low-frequency features, according to low-resolution images of different inputs. To obtain complementary low-frequency features, a 16-layer symmetrical lower network is designed. It depends on a symmetrical architecture to enhance inter hierarchical connections to obtain more complementary structural information. Also, two sub-networks can interact information via a multiplication operation. A 2-layer construction block is used to transform low-frequency features to high-frequency features and construct predicted high-quality images. The process can be illustrated via the following formulates.

$$\begin{aligned}
 I_S &= ADSRNet(I_L) \\
 &= CB(HUNet(I_L) \times SLNet(I_L)) \\
 &= CB((5HB(CR(I_L))) \times SLNet(I_L)) \\
 &= CB(O_{HUNet} \times O_{SLNet}),
 \end{aligned} \tag{1}$$

where *ADSRNet*, *HUNet* and *SLNet* are used as *ADSRNet*, heterogeneous upper network and symmetrical lower network, respectively. *CR* is a CRU. *5HB* is five stacked heterogeneous blocks. *CB* denotes a construction block. \times represents multiplication operation. Parameters of obtained *ADSRNet* can be obtained via a loss function in Section III. *B*. O_{HUNet} and O_{SLNet} are outputs of the *HUNet* and *SLNet*, respectively. I_L and I_S represent the input low-resolution image and the output high-resolution image, respectively.

B. Loss Function

ADSRNet choose mean absolute error (MAE) [36] as the loss function to obtain parameters. Work process of MAE in the *ADSRNet* can be represented as below.

$$l(p) = 1/T \sum_{j=1}^T \left| ADSRNet(I_L^j) - I_H^j \right|, \quad (2)$$

where I_L^j and I_H^j denote the j th low- and high-resolution images, respectively. *ADSRNet* denote function of *ADSRNet*, respectively. T represents the number of low-resolution images. l is a loss function of *ADSRNet*. Also, p stands for parameters of the trained *ADSRNet*. Also, it can be optimized by the Adam optimizer [37].

C. Heterogeneous Block

To improve the SISR effect and robustness of the network, heterogeneous blocks are conducted to dynamically adjust parameters to obtain robust low-frequency information, according to different input low-resolution images. Each heterogeneous block is composed of a dilated CRU, dynamic CRU and CRU, where dilated CRU represents a combination of a dilated convolution [38] and a ReLU [39]. That is used to capture more context information. A dynamic CRU is a combination of a dynamic convolution [29] and ReLU, where can adaptively learn parameters, according to different input information. To resolve long-term dependency, a RL operation is employed between an input of a dilated CRU and output of CRU. Mentioned convolutional kernels are 3×3 . Input channel number and output channel number, i.e., dilated, dynamic and common convolutional layers are 64. Also, dilated factor is 2 in the dilated convolutional layers. The mentioned process can be conducted the following equation.

$$HB(O_t) = CR(DyCR(DiCR(O_t))) + O_t, \quad (3)$$

where O_t is used to define an input of a heterogeneous block. *CR* is a CRU. *DiCR* stands for a dilated CRU. *DyCR* represents a dynamic CRU. $+$ is used to express a RL operation also regarded to \oplus in Fig. 1.

D. Symmetrical Lower Sub-network

To obtain complementary low-frequency information, a 16-layer symmetrical lower network is conducted. Each layer contains a CRU, where its channel number of input and output are 64 besides the first layer, its kernel is 3×3 . Channel number of input and output from the first layer are set to 3 and 64,

respectively. To enhance relations of different layers, residual learning operations are used to act between the 1st and 16th, the 2nd and 15th, 3rd and 14th, 4th and 13th, 5th and 12th, 6th and 11th, 7th and 10th, 8th and 9th layers to transfer obtained information of shallow layers to deep layers to prevent long-term dependency and obtain robust information for SISR. The procedure can be summarized as Eq. (4).

$$O_{SLNet} = CR(CR(\dots(CR(CR(O_8 + CR(O_8)) + O_7) + O_6) + \dots) + O_2) + O_1, \quad (4)$$

where O_i denotes an output of the i th layer and $i = 1, 2, 3, \dots, 8$. Also, $O_i = iCR(I_L)$, where iCR stands for i stacked CRU. O_{SLNet} represent the output of *SLNet*, respectively.

E. Construction Block

A 2-layer construction block is used to construct predicted HR images. It includes two steps. The first step is acted to a sub-pixel convolutional layer, which can use low-frequency features to obtain high-frequency features. Its input and output channel number are 128 and 64, respectively. The second phase only utilizes a convolutional layer (Conv) to construct predicted resolution images, where its input and output channel number are 64 and 3, respectively. Their kernel sizes are 3×3 . These illustrations can be symbolled as Eq. (5).

$$O_S = CB(O_{HUNet} \times O_{SLNet}) \\ = C(Sub(O_{HUNet} \times O_{SLNet})), \quad (5)$$

where *Sub* and *C* are functions of a sub-pixel convolutional layer and a convolutional layer, respectively. *CB* denotes a construction block. O_{HUNet} and O_{SLNet} express the output of *HUNet* and *SLNet*.

IV. EXPERIMENTS

A. Training Dataset

We utilize the public DIV2K dataset [40] as a training set to develop a *ADSRNet* for enhancing image super-resolution capabilities. Specifically, the DIV2K contains three parts, i.e., a training dataset containing 800 images, a validation dataset containing 100 images and a test dataset containing 100 images. To enlarge diversity of a training dataset, we merge an original dataset and a validation dataset to form a new training dataset, which includes 900 high-quality images and corresponding LR images of x2, x3 and x4. All training images are saved format of ‘.png’.

B. Test Datasets

To fairly test SR performance of our *ADSRNet*, four public SR datasets, i.e., Set5 containing 5 natural images [41], Set14 containing 14 natural images [42], BSD100 (B100) containing 100 natural images [43] and Urban100 (U100) containing 100 containing [44] are used to conduct experiments. These datasets include three different scales, i.e., x2, x3 and x4. They are saved as format of ‘.png’.

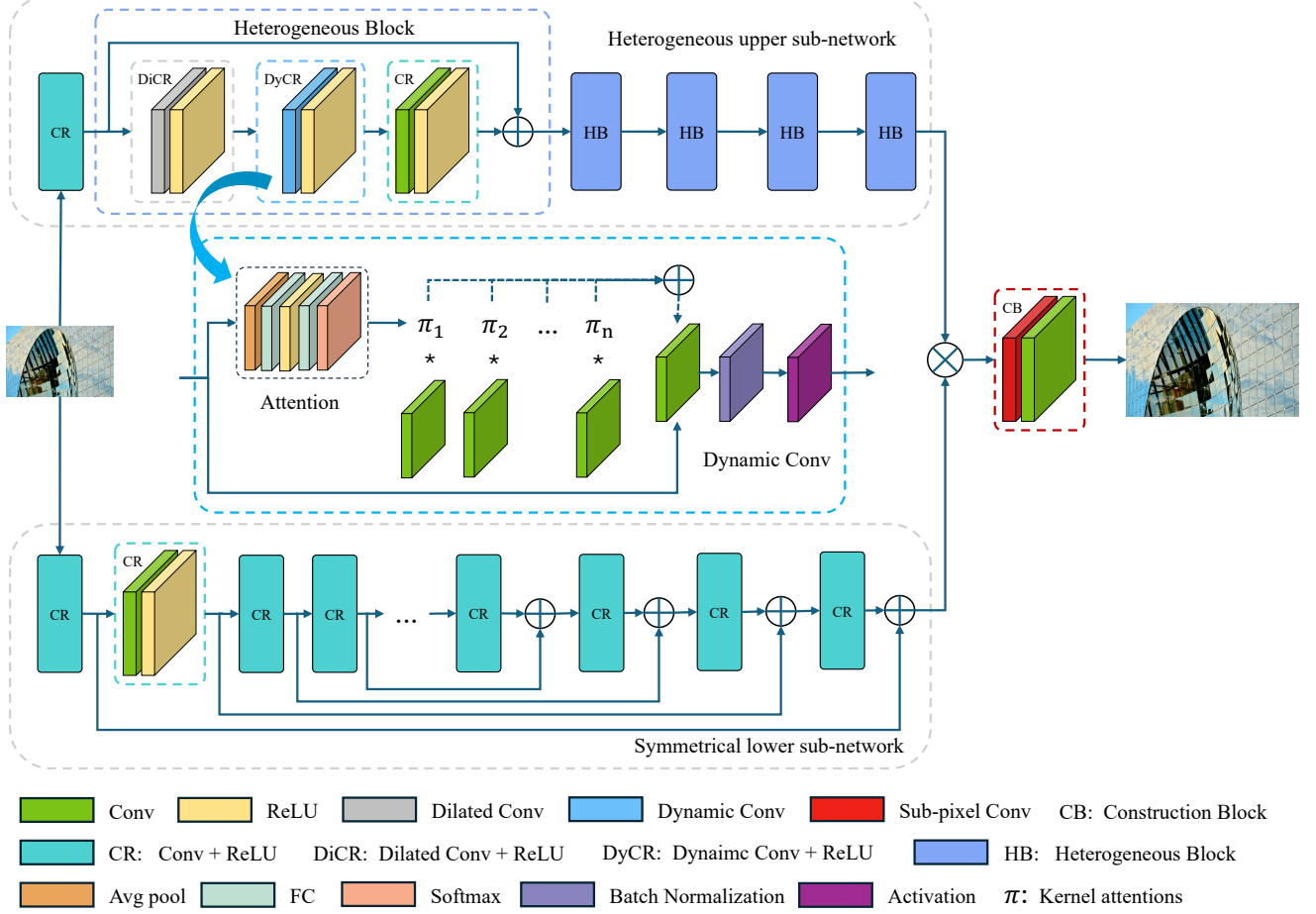


Fig. 1. Network architecture of the proposed ADSRNet.

C. Implementation Details

Original parameters of training a ADSRNet are β_1 of 0.9, β_2 of 0.999, epsilon of 1e-8, batch size of 64 and initial learning rate of 1e-4, which is halved every 300,000 steps. Also, it more parameters are the same as Ref. [22].

The proposed ADSRNet is developed based on Pytorch 1.8.0 and Python 3.8. And all the experiments run on a workstation with Ubuntu 20.04, which equipped AMD EPYC 7502P CPU and four GPUs of Nvidia GeForce RTX 3090 with Nvidia CUDA 11.1, and cuDNN 8005. All experiments are trained via one 3090 GPU.

D. Network Analysis

We analyze architecture of designed ADSRNet containing a heterogeneous upper sub-network, symmetrical lower-network and construction block for image super-resolution, according to its rationality and validity.

Heterogeneous upper sub-network: Most of existing SR models cannot adaptively learn parameters, according to different given low-resolution images [45]. Dynamic convolutions can automatically adjust parameters, according to different inputs [29]. In response to this motivation, we have developed a heterogeneous upper sub-network specifically for image

super-resolution. A heterogeneous network architecture can facilitate more diversified structural information, which can provide complementary information to strengthen robustness of an obtained SISR model. Efficient super-resolution performance of proposed ADSRNet is implemented by enhancing relation of context information, salient information relation of a kernel mapping and relations of shallow and deep layers. That is, dilated convolutions are used to enhance relations of context information for SISR. Dynamic convolutions are used to enhance relations of salient information in a kernel mapping to improve adaptive ability of obtained ADSRNet. Also, residual learning technique is used to enhance relations of shallow and deep layers to prevent long-term dependency issue for SISR. More detailed design of the heterogeneous upper sub-network is given as follows. We design a main network, according to VGG [46]. That is, six stacked CRU is used as a basic network to extract structural low-frequency information. A combination of six stacked CRU and a CB has obtained peak signal-to-noise ratio (PSNR) [47] of 25.13dB and structural similarity (SSIM) [47] of 0.7525 on U100 for x4, which shows effectiveness of six stacked CRU. A CB is used to build HR images, which can be shown in latter section. To prevent long-term dependency problem, deep fusion idea [48] is used in this paper. That is, each RL operation is used to

TABLE I
SISR RESULTS OF DIFFERENT METHODS ON U100 FOR x4.

Scale	Methods	PSNR(dB)/SSIM
x4	A combination of six stacked CRU and a CB	25.13/0.7525
	Heterogeneous upper sub-network without Dilated CRU, Dynamic CRU and a CB	25.22/0.7559
	Heterogeneous upper sub-network without dynamic CRU and a CB	25.46/0.7649
	Heterogeneous upper sub-network without dilated CRU and a CB	25.61/0.7697
	Heterogeneous upper sub-network with CRU rather than dilated CRU	25.74/0.7739
	Heterogeneous upper sub-network with CRU rather than dynamic CRU	25.68/0.7729
	Heterogeneous upper sub-network and a CB	25.75/0.7740
	ADSRNet without residual learning operations in symmetrical lower sub-network	25.99/0.7825
	ADSRNet	26.01/0.7827

act between an input and output of CRU besides the first CRU to transform low-frequency information from shallow layers to deep layers to pursue better performance on super-resolution. Its effectiveness can be shown by comparing ‘Heterogeneous upper sub-network without Dilated CRU, Dynamic CRU and a CB’ and ‘A combination of six stacked Conv’ in terms of PSNR and SSIM in TABLE I. To extract more context, each dilated CRU with dilated factor of 2 is used before each CRU besides the first CRU in heterogeneous upper sub-network. Its effectiveness can be proved by comparing ‘Heterogeneous upper sub-network without Dilated CRU, Dynamic CRU and a CB’ and ‘Heterogeneous upper sub-network without dynamic CRU and a CB’ in terms of PSNR and SSIM on U100 for x4. Specifically, five stacked blocks besides the first CRU in the heterogeneous upper sub-network (HUNet) are five heterogeneous blocks (HBs) rationality and validity are shown in latter section. To make HUNet robust, each Dynamic CRU is set behind each Dilated CRU in each HB to dynamically adjust parameters, according to different inputs. Its better SR results can be found via comparing ‘Heterogeneous upper sub-network and a CB’ and ‘Heterogeneous upper sub-network without dynamic CRU and a CB’ in TABLE I, where effectiveness of dynamic convolutions is verified. It is known that difference of network architecture is bigger, its performance is better [28]. Motivated by that, we respectively use CRU rather than Dynamic CRU and Dilated CRU to conduct experiments. TABLE I shows that ‘Heterogeneous upper sub-network and a CB’ has obtained higher PSNR and SSIM values than that of ‘Heterogeneous upper sub-network with CRU rather than dilated CRU’ and ‘Heterogeneous upper sub-network with CRU rather than dynamic CRU’. This approach demonstrates the effectiveness of dynamic CRU and dilated CRU in HB, and highlights the advantages of various network architectures within HB for image super-resolution.

Symmetrical lower sub-network: To prevent poor representation of single network for image super-resolution, a symmetrical lower sub-network is designed, which can be used to assist an upper network to extract more complementary structural information to improve recovered high-resolution images. That is implemented by the following phases.

The first phase design a 16-layer stacked CRU to extract low-frequency structural information, according to VGG [46].

TABLE II
SISR RESULTS OF DIFFERENT METHODS WITH ON SET5 FOR THREE UPSCALE FACTORS.

Dataset	Methods	x2	x3	x4
		PSNR(dB)/SSIM	PSNR(dB)/SSIM	PSNR(dB)/SSIM
Set5	Bicubic	33.66/0.9299	30.39/0.8682	28.42/0.8104
	SRCNN [15]	36.66/0.9542	32.75/0.9090	30.48/0.8628
	VDSR [16]	37.53/0.9587	33.66/0.9213	31.35/0.8838
	DRRN [18]	37.74/0.9591	34.03/0.9244	31.68/0.8888
	FSRCNN [21]	37.00/0.9558	33.16/0.9140	30.71/0.8657
	CARN-M [26]	37.53/0.9583	33.99/0.9236	31.92/0.8903
	IDN [36]	37.83/0.9600	34.11/0.9253	31.82/0.8903
	A+ [49]	36.54/0.9544	32.58/0.9088	30.28/0.8603
	JOR [50]	36.58/0.9543	32.55/0.9067	30.19/0.8563
	RFL [51]	36.54/0.9537	32.43/0.9057	30.14/0.8548
	SelfEx [44]	36.49/0.9537	32.58/0.9093	30.31/0.8619
	CSCN [52]	36.93/0.9552	33.10/0.9144	30.86/0.8732
	RED [53]	37.56/0.9595	33.70/0.9222	31.33/0.8847
	DnCNN [54]	37.58/0.9590	33.75/0.9222	31.40/0.8845
	TNRD [55]	36.86/0.9556	33.18/0.9152	30.85/0.8732
	FDSR [56]	37.40/0.9513	33.68/0.9096	31.28/0.8658
	RCN [57]	37.17/0.9583	33.45/0.9175	31.11/0.8736
	DRCN [17]	37.63/0.9588	33.82/0.9226	31.53/0.8854
	LapSRN [58]	37.52/0.9590	-	31.54/0.8850
	NDRCN [59]	37.73/0.9596	33.90/0.9235	31.50/0.8859
	MemNet [25]	37.78/0.9597	34.09/0.9248	31.74/0.8893
	LESRCNN [60]	37.65/0.9586	33.93/0.9231	31.88/0.8903
	LESRCNN-S [60]	37.57/0.9582	34.05/0.9238	31.88/0.8907
	ScSR [61]	35.78/0.9485	31.34/0.8869	29.07/0.8263
	DSRCNN [62]	37.73/0.9588	34.17/0.9247	31.89/0.8909
	DAN [63]	37.34/0.9526	34.04/0.9199	31.89/0.8864
	PGAN [64]	-	-	31.03/0.8798
	ADSRNet (Ours)	37.95/0.9604	34.31/0.9263	32.15/0.8927

TABLE III
SISR RESULTS OF DIFFERENT METHODS ON SET14 FOR THREE UPSCALE FACTORS.

Dataset	Methods	x2	x3	x4
		PSNR(dB)/SSIM	PSNR(dB)/SSIM	PSNR(dB)/SSIM
Set14	Bicubic	30.24/0.8688	27.55/0.7742	26.00/0.7027
	SRCNN [15]	32.42/0.9063	29.28/0.8209	27.49/0.7503
	VDSR [16]	33.03/0.9124	29.77/0.8314	28.01/0.7674
	DRRN [18]	33.23/0.9136	29.96/0.8349	28.21/0.7720
	FSRCNN [21]	32.63/0.9088	29.43/0.8242	27.59/0.7535
	CARN-M [26]	33.26/0.9141	30.08/0.8367	28.42/0.7762
	IDN [36]	33.30/0.9148	29.99/0.8354	28.25/0.7730
	A+ [49]	32.28/0.9056	29.13/0.8188	27.32/0.7491
	JOR [50]	32.38/0.9063	29.19/0.8204	27.27/0.7479
	RFL [51]	32.26/0.9040	29.05/0.8164	27.24/0.7451
	SelfEx [44]	32.22/0.9034	29.16/0.8196	27.40/0.7518
	CSCN [52]	32.56/0.9074	29.41/0.8238	27.64/0.7578
	RED [53]	32.81/0.9135	29.50/0.8334	27.72/0.7698
	DnCNN [54]	33.03/0.9128	29.81/0.8321	28.04/0.7672
	TNRD [55]	32.51/0.9069	29.43/0.8232	27.66/0.7563
	FDSR [56]	33.00/0.9042	29.61/0.8179	27.86/0.7500
	RCN [57]	32.77/0.9109	29.63/0.8269	27.79/0.7594
	DRCN [17]	33.04/0.9118	29.76/0.8311	28.02/0.7670
	LapSRN [58]	33.08/0.9130	29.63/0.8269	28.19/0.7720
	NDRCN [59]	33.20/0.9141	29.88/0.8333	28.10/0.7697
	MemNet [25]	33.28/0.9142	30.00/0.8350	28.26/0.7723
	LESRCNN [60]	33.32/0.9148	30.12/0.8380	28.44/0.7772
	LESRCNN-S [60]	33.30/0.9145	30.16/0.8384	28.43/0.7776
	ScSR [61]	31.64/0.8940	28.19/0.7977	26.40/0.7218
	DSRCNN [62]	33.43/0.9157	30.24/0.8402	28.46/0.7796
	DAN [63]	33.08/0.9041	30.09/0.8287	28.42/0.7687
	PGAN [64]	-	-	27.75/0.8164
	ADSRNet (Ours)	33.52/0.9170	30.27/0.8412	28.56/0.7799

Its effectiveness can be proved via ‘Heterogeneous upper sub-network and a CB’ and ‘ADSRNet without RL operations in symmetrical lower sub-network’ in TABLE I. To enhance relationship of hierarchical features, the second phase is conducted. It uses RL operations to gather obtained features of shallow and deep layers to achieve a symmetrical lower sub-network to extract more accurate information as shown in Section III.D. As illustrated in TABLE I, we can see that

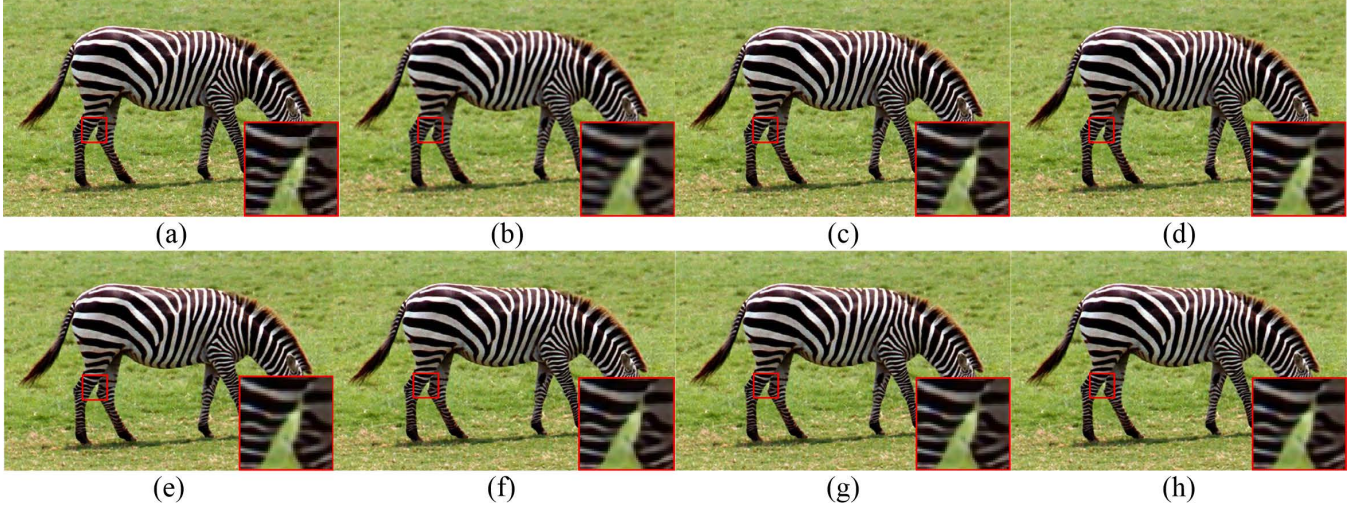


Fig. 2. Predicted high-quality images from different methods on a same low-resolution image from Set14 for $\times 2$: (a) A HR image, (b) Bicubic, (c) SRCNN, (d) LESRCNN, (e) DCLS, (f) VDSR, (g) DRCN and (h) ADSRNet (Ours).

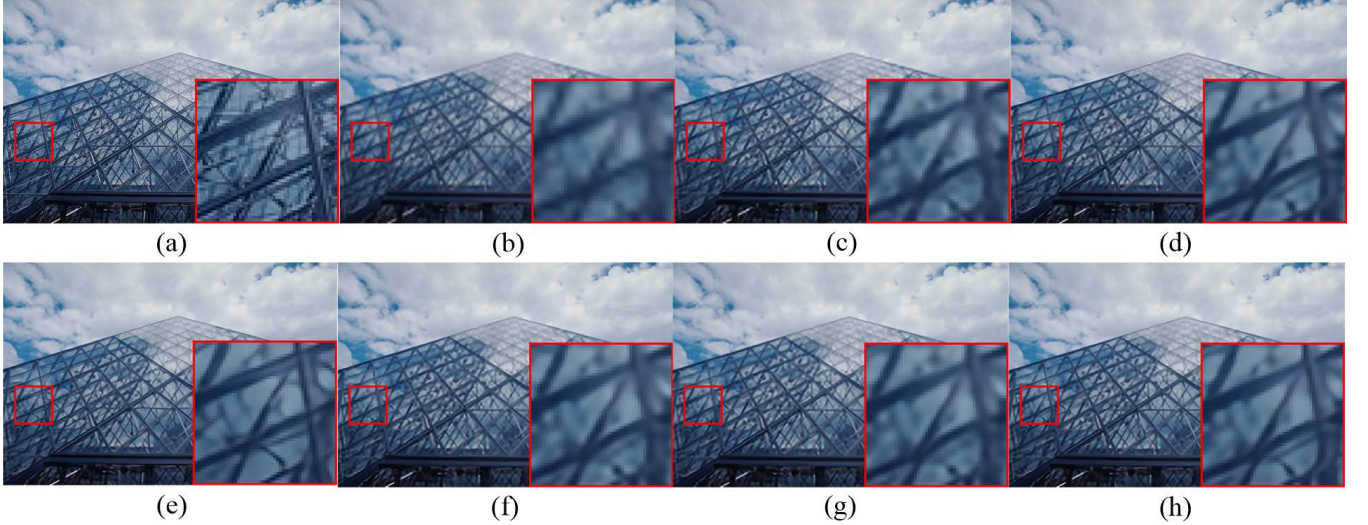


Fig. 3. Predicted high-quality images from different methods on a same low-resolution image from B100 for $\times 3$: (a) A HR image, (b) Bicubic, (c) SRCNN, (d) LESRCNN, (e) DCLS, (f) VDSR, (g) DRCN and (h) ADSRNet (Ours).

'ADSRNet' has obtained higher PSNR and SSIM than that of ADSRNet without RL operations in symmetrical lower sub-network, which shows effectiveness of RL operations in the symmetrical lower sub-network for image SR. Besides, 'ADSRNet' has obtained higher PSNR value than that of 'Heterogeneous upper sub-network and a CB' in TABLE I, which shows effectiveness of Heterogeneous parallel networks for image super-resolution.

Construction block: To construct HR images, we design a 2-layer construction block. It consists of a sub-pixel convolutional layer and a convolutional layer. Sub-pixel convolutional layer is used to amplify low-frequency features to high-frequency features. A convolutional layer is utilized to construct predicted HR images.

E. Comparisons with Popular Methods for SR

A heterogeneous network architecture can more diversified structural information, which can provide complementary information to strengthen robustness of an obtained SISR model. The heterogeneous network is deigned, according to enhancing relation of context information, salient information relation of a kernel mapping and relations of shallow and deep layers. Besides, a deep network via parallel networks can extract extra structural information to facilitate more representative information to further improve SR effect. These make our ADSRNet obtain better SR results than these of some classical SR methods, i.e., VDSR [16], DRCN [17]. Rationality and effectiveness of key techniques in our ADSRNet are given in Section IV. D. Superiority of the proposed ADSRNet for SISR is given as follows. In this section, we use both quantitative and qualitative analysis to evaluate results of our ADSRNet on SISR. Quantitative analysis includes PSNR, SSIM, running

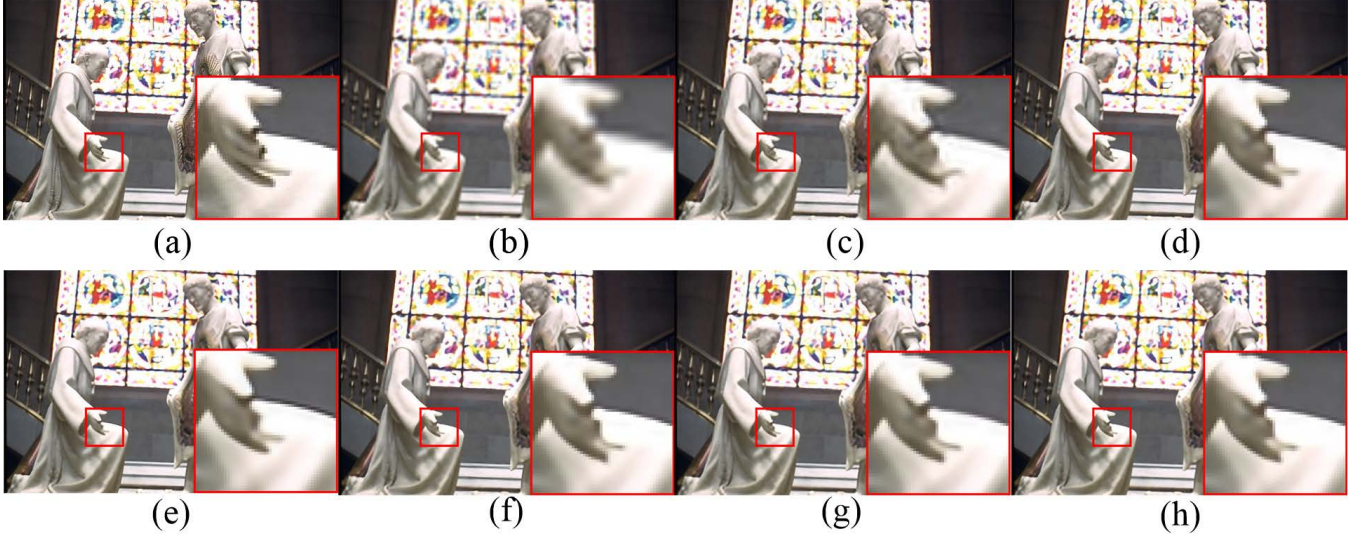


Fig. 4. Predicted high-quality images from different methods on a same low-resolution image from B100 for $\times 3$: (a) A HR image, (b)Bicubic, (c) SRCNN, (d) LESRCNN, (e) DCLS, (f) VDSR, (g) DRCN and (h) ADSRNet (Ours).

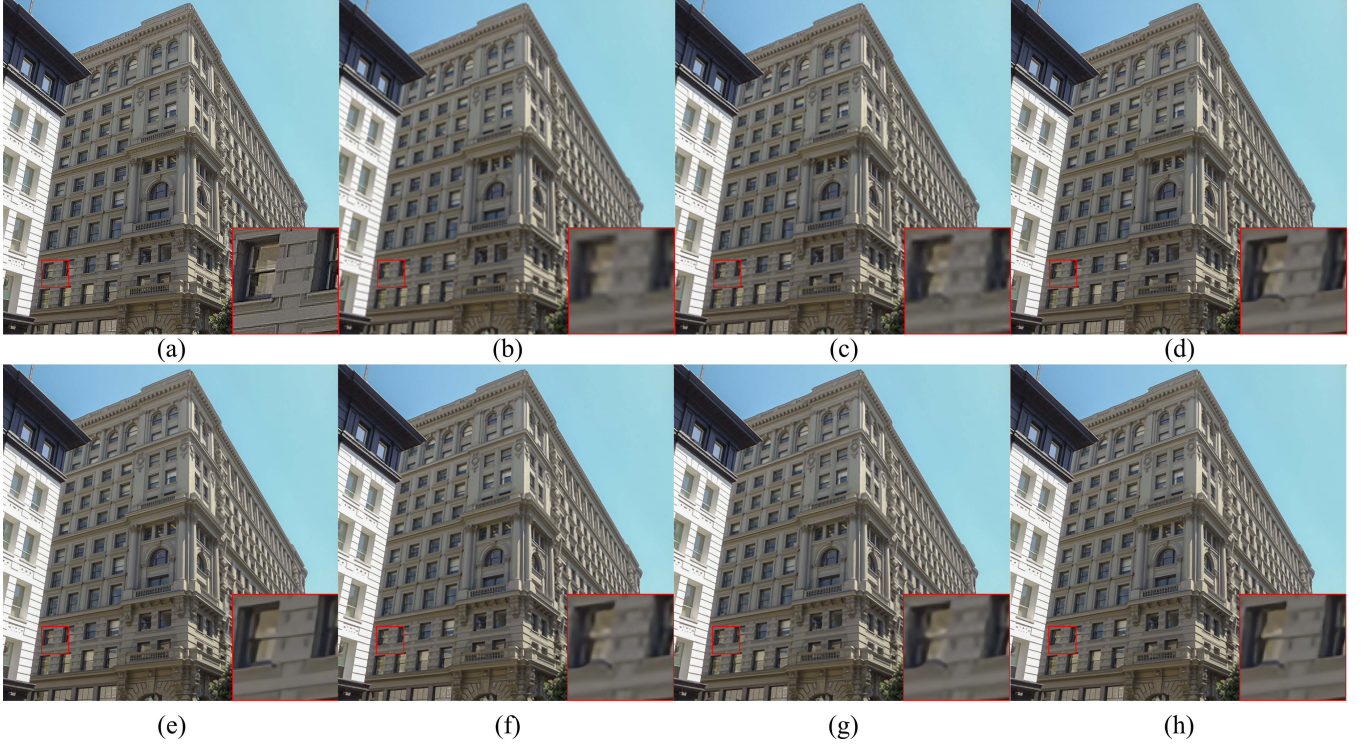


Fig. 5. Predicted high-quality images from different methods on a same low-resolution image from U100 for $\times 4$: (a) A HR image, (b)Bicubic, (c) SRCNN, (d) LESRCNN, (e) DCLS, (f) VDSR, (g) DRCN and (h) ADSRNet (Ours).

time and complexity of our ADSRNet. Specifically, PSNR and SSIM are used to measure quality of predicted HR images. Also, running time and parameters are used to test feasibility of our ADSRNet for real applications, i.e., phones and cameras. We use A+ [49], jointly optimized regressors (JOR) [50], image upscaling with super-resolution forests (RFL) [51], self-exemplars SR method (SelfEx) [44], cascade of sparse coding based network (CSCN) [52], image restoration using encoder-decoder networks (RED) [53], denoising convolutional neural

network (DnCNN) [54], trainable non-linear reaction diffusion (TNRD) [55], fast dilated residual SR convolutional network (FDSR) [56], SRCNN [15], FSRCNN [21], residue context sub-network (RCN) [57], VDSR [16], DRCN [17], IDN [36], DRRN [18], Laplacian SR network (LapSRN) [58], new architecture of deep recursive convolution networks for SR (NDRCN) [59], a persistent memory network (MemNet) [25], CARN-M [26], light-weight image super-resolution with enhanced CNN (LESRCNN) [60], deep alternating network

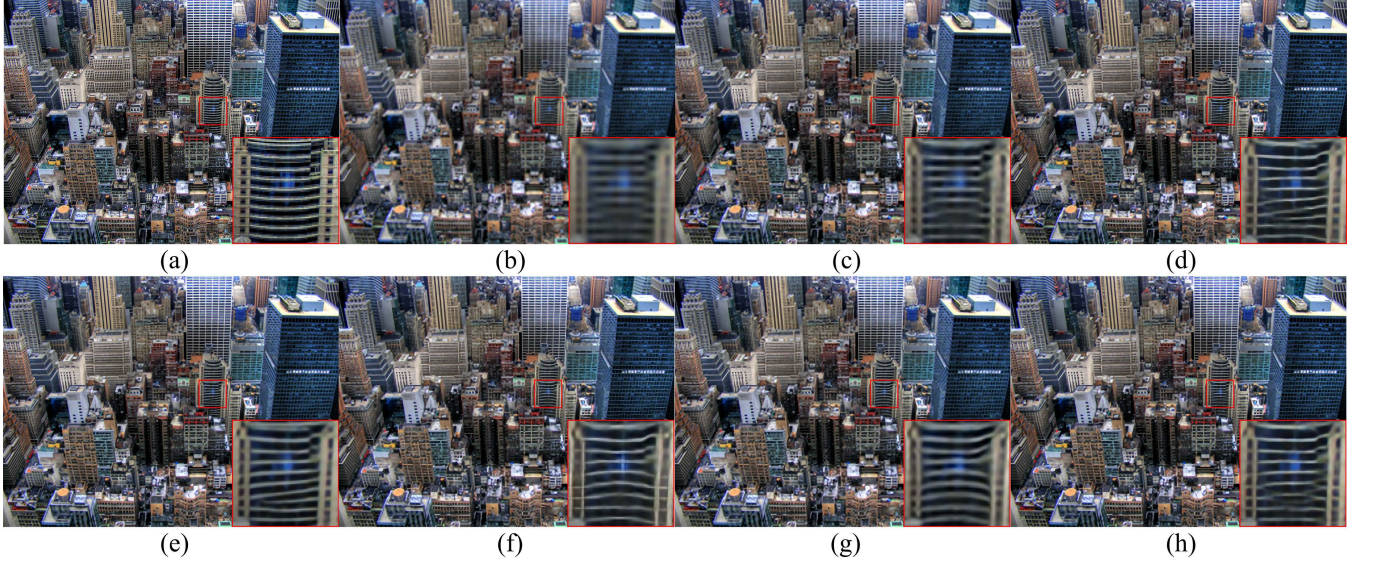


Fig. 6. Predicted high-quality images from different methods on a same low-resolution image from U100 for $\times 4$: (a) A HR image, (b) Bicubic, (c) SRCNN, (d) LESRCNN, (e) DCLS, (f) VDSR, (g) DRCN and (h) ADSRNet (Ours).

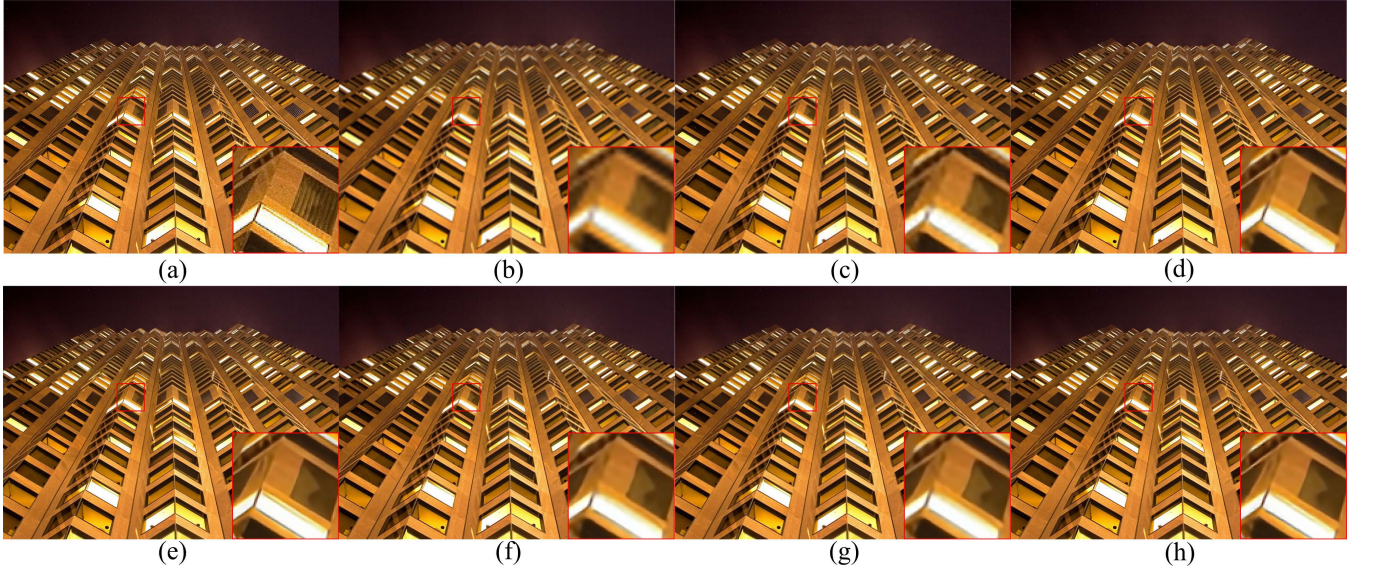


Fig. 7. Predicted high-quality images from different methods on a same low-resolution image from U100 for $\times 4$: (a) A HR image, (b) Bicubic, (c) SRCNN, (d) LESRCNN, (e) DCLS, (f) VDSR, (g) DRCN and (h) ADSRNet (Ours).

(DAN) [63], Pixel-Level Generative Adversarial Network (PGAN) [64] and our ADSRNet on four public datasets, i.e., Set5, Set14, B100 and U100 for $\times 2$, $\times 3$ and $\times 4$ to conduct experiments. As shown in TABLEs II and III, we can see that our ADSRNet has obtained the best performance in terms of PSNR and SSIM for $\times 2$, $\times 3$ and $\times 4$. For instance, our ADSRNet has improvements of 0.12dB on PSNR and 0.004 on SSIM on Set 5 for $\times 2$ than that of IDN in TABLE II. Our ADSRNet has obtained improvements of 0.1dB on PSNR and 0.003 on SSIM on Set14 for $\times 4$ than that of DSRCNN in TABLE III. That also shows that our ADSRNet is effective on small datasets for image super-resolution. For big datasets, our ADSRNet still has an advantage for image super-resolution in TABLEs IV and V, we can see that our ADSRNet has obtained

the best SR results for all the scale factors, i.e., $\times 2$, $\times 3$ and $\times 4$. For instance, our ADSRNet has exceeded 0.09dB on PSNR and 0.0016 on SSIM than that of DSRCNN for $\times 2$ on B100 in TABLE IV. Our ADSRNet has exceeded 0.07dB on PSNR and 0.0012 on SSIM than that of DSRCNN for $\times 4$ on U100 in TABLE V. That shows that our ADSRNet is suitable to big datasets for image super-resolution. Specifically, red and blue lines denote the best and second SR results from TABLE II to TABLE V, respectively.

To test practicality of our ADSRNet, we use running time and complexity to test performance of our ADSRNet for image SR. As shown in TABLE VI, our ADSRNet has obtained competitive running time for restoring LR images sizes of 256×256 and 512×512 . As illustrated in TABLE

TABLE IV
SISR RESULTS OF DIFFERENT METHODS ON B100 FOR THREE UPSCALE FACTORS.

Dataset	Methods	x2		x3		x4	
		PSNR(dB)/SSIM	PSNR(dB)/SSIM	PSNR(dB)/SSIM	PSNR(dB)/SSIM	PSNR(dB)/SSIM	PSNR(dB)/SSIM
B100	Bicubic	29.56/0.8431		27.21/0.7385		25.96/0.6675	
	SRCNN [15]	31.36/0.8879		28.41/0.7863		26.90/0.7101	
	VDSR [16]	31.90/0.8960		28.82/0.7976		27.29/0.7251	
	DRRN [18]	32.05/0.8973		28.95/0.8004		27.38/0.7284	
	FSRCNN [21]	31.53/0.8920		28.53/0.7910		26.98/0.7150	
	CARN-M [26]	31.92/0.8960		28.91/0.8000		27.44/0.7304	
	IDN [36]	32.08/0.8985		28.95/0.8013		27.41/0.7297	
	A+ [49]	31.21/0.8863		28.29/0.7835		26.82/0.7087	
	JOR [50]	31.22/0.8867		28.27/0.7837		26.79/0.7083	
	RFL [51]	31.16/0.8840		28.22/0.7806		26.75/0.7054	
	SelfEx [44]	31.18/0.8855		28.29/0.7840		26.84/0.7106	
	CSCN [52]	31.40/0.8884		28.50/0.7885		27.03/0.7161	
	RED [53]	31.96/0.8972		28.88/0.7993		27.35/0.7276	
	DnCNN [54]	31.90/0.8961		28.85/0.7981		27.29/0.7253	
	TNRD [55]	31.40/0.8878		28.50/0.7881		27.00/0.7140	
	FDSR [56]	31.87/0.8847		28.82/0.7797		27.31/0.7031	
	DRCN [17]	31.85/0.8942		28.80/0.7963		27.23/0.7233	
	LapSRN [58]	31.80/0.8950		-		27.32/0.7280	
	NDRCN [59]	32.00/0.8975		28.86/0.7991		27.30/0.7263	
	MemNet [25]	32.08/0.8978		28.96/0.8001		27.40/0.7281	
	LESRCNN [60]	31.95/0.8964		28.91/0.8005		27.45/0.7313	
	LESRCNN-S [60]	31.95/0.8965		28.94/0.8012		27.47/0.7321	
	ScSR [61]	30.77/0.8744		27.72/0.7647		26.61/0.6983	
	DSRCNN [62]	32.05/0.8978		29.01/0.8029		27.50/0.7341	
	DAN [63]	31.76/0.8858		28.94/0.7919		27.51/0.7248	
	PGAN [64]	-		-		26.35/0.6926	
	ADSRNet (Ours)	32.14/0.8994		29.06/0.8048		27.55/0.7357	

TABLE V
SISR RESULTS OF DIFFERENT METHODS ON U100 FOR THREE UPSCALE FACTORS.

Dataset	Methods	x2		x3		x4	
		PSNR(dB)/SSIM	PSNR(dB)/SSIM	PSNR(dB)/SSIM	PSNR(dB)/SSIM	PSNR(dB)/SSIM	PSNR(dB)/SSIM
U100	Bicubic	26.88/0.8403		24.46/0.7349		23.14/0.6577	
	SRCNN [15]	29.50/0.8946		26.24/0.7989		24.52/0.7221	
	VDSR [16]	30.76/0.9140		27.14/0.8279		25.18/0.7524	
	DRRN [18]	31.23/0.9188		27.53/0.8378		25.44/0.7638	
	FSRCNN [21]	29.88/0.9020		26.43/0.8080		24.62/0.7280	
	CARN-M [26]	31.23/0.9193		27.55/0.8385		25.62/0.7694	
	IDN [36]	31.27/0.9196		27.42/0.8359		25.41/0.7632	
	A+ [49]	29.20/0.8938		26.03/0.7973		24.32/0.7183	
	JOR [50]	29.25/0.8951		25.97/0.7972		24.29/0.7181	
	RFL [51]	29.11/0.8904		25.86/0.7900		24.19/0.7096	
	SelfEx [44]	29.54/0.8967		26.44/0.8088		24.79/0.7374	
	RED [53]	30.91/0.9159		27.31/0.8303		25.35/0.7587	
	DnCNN [54]	30.74/0.9139		27.15/0.8276		25.20/0.7521	
	TNRD [55]	29.70/0.8994		26.42/0.8076		24.61/0.7291	
	FDSR [56]	30.91/0.9088		27.23/0.8190		25.27/0.7417	
	DRCN [17]	30.75/0.9133		27.15/0.8276		25.14/0.7510	
	LapSRN [58]	30.41/0.9100		-		25.21/0.7560	
	WaveResNet [65]	30.96/0.9169		27.28/0.8334		25.36/0.7614	
	CPCA [66]	28.17/0.8990		25.61/0.8123		23.62/0.7257	
	NDRCN [59]	31.06/0.9175		27.23/0.8312		25.16/0.7546	
	MemNet [25]	31.31/0.9195		27.56/0.8376		25.50/0.7630	
	LESRCNN [60]	31.45/0.9206		27.70/0.8415		25.77/0.7732	
	LESRCNN-S [60]	31.45/0.9207		27.76/0.8424		25.78/0.7739	
	ScSR [61]	28.26/0.8828		-		24.02/0.7024	
	DSRCNN [62]	31.83/0.9252		27.99/0.8483		25.94/0.7815	
	DAN [63]	30.60/0.9060		27.65/0.8352		25.86/0.7721	
	LDRAN [67]	-		-		25.91/0.7786	
	PGAN [64]	-		-		25.47/0.9574	
	ADSRNet (Ours)	32.00/0.9267		28.02/0.8493		26.01/0.7827	

TABLE VI
RUNNING TIME (MILLISECOND) OF DIFFERENT METHODS FOR IMAGE SUPER-RESOLUTION VIA DIFFERENT SIZES FOR $\times 4$.

Image sizes	VDSR [16]	CARN-M [26]	ACNet [68]	ADSRNet (Ours)
256 \times 256	17.2	15.9	18.38	14.17
512 \times 512	57.5	19.9	75.79	26.11

VII, although our ADSRNet has obtained more parameters

TABLE VII
PARAMETERS AND FLOPS OF DIFFERENT METHODS WITH SCALE FACTOR OF 4 FOR RESTORATION HIGH-QUALITY IMAGES OF 1024 \times 1024.

Methods	Parameters	Flops
DCLS [69]	13,626K	498.18G
ACNet [68]	1,357K	132.82G
ADSRNet (Ours)	1,819K	110.99G

than that of ACNet, it has obtained less flops than that of ACNet. Thus, it is competitive in complexity and suitable for application in consumer electronic products. According to experiment results, our ADSRNet is effective in terms of quantitative analysis.

For qualitative analysis, we use Bicubic, SRCNN, LESRCNN, DCLS, VDSR, DRCN and ADSRNet on a low-resolution image from the B100 and U100 for x3 and x4 to recover high-quality images, which are used to compare with given HR images. That is, we amplify one area of predicted high-quality images from different methods as observation areas, observation areas are clearer, their corresponding methods are more effective for SISR. As shown in Figs.2-7, our ADSRNet has obtained clearer areas, it shows that our ADSRNet is effective for qualitative analysis. In a summary, our ADSRNet is a good tool for image resolution, according to quantitative and qualitative analysis.

V. CONCLUSION

In this paper, we propose a adaptive convolutional network via a parallel network in SISR. The upper network depends on enhancing relation of context information, salient information relation of a kernel mapping and relations of shallow and deep layers to implement efficient SR performance. The lower network relies on a symmetric architecture to strengthen relation of hierarchical information to improve effect of SISR. Two networks can extract complementary information to facilitate more robust information to protect performance of SISR for different scenes. We will deal with SISR with non-reference images in the future.

REFERENCES

- [1] Z. Zha, X. Yuan, B. Wen, J. Zhou, J. Zhang, and C. Zhu, "From rank estimation to rank approximation: Rank residual constraint for image restoration," *IEEE Transactions on Image Processing*, vol. 29, pp. 3254–3269, 2019.
- [2] F. Zhou, W. Yang, and Q. Liao, "Single image super-resolution using incoherent sub-dictionaries learning," *IEEE Transactions on Consumer Electronics*, vol. 58, no. 3, pp. 891–897, 2012.
- [3] S. Wang and Y. Zhang, "Deep learning for covid-19 diagnosis via chest images," *Computers, Materials & Continua*, vol. 76, no. 1, pp. 129–132, 2023.
- [4] X. Zhou, X. Zheng, T. Shu, W. Liang, I. Kevin, K. Wang, L. Qi, S. Shimizu, and Q. Jin, "Information theoretic learning-enhanced dual-generative adversarial networks with causal representation for robust ood generalization," *IEEE Transactions on Neural Networks and Learning Systems*, 2023.
- [5] Q. Zhu, B. Xu, J. Huang, H. Wang, R. Xu, W. Shao, and D. Zhang, "Deep multi-modal discriminative and interpretability network for alzheimer's disease diagnosis," *IEEE Transactions on Medical Imaging*, vol. 42, no. 5, pp. 1472–1483, 2022.
- [6] Y. Zhang, L. Deng, H. Zhu, W. Wang, Z. Ren, Q. Zhou, S. Lu, S. Sun, Z. Zhu, J. M. Gorri *et al.*, "Deep learning in food category recognition," *Information Fusion*, vol. 98, p. 101859, 2023.

[7] Y.-D. Zhang, Z. Dong, S.-H. Wang, X. Yu, X. Yao, Q. Zhou, H. Hu, M. Li, C. Jiménez-Mesa, J. Ramirez *et al.*, “Advances in multimodal data fusion in neuroimaging: overview, challenges, and novel orientation,” *Information Fusion*, vol. 64, pp. 149–187, 2020.

[8] X. Zhou, Q. Yang, Q. Liu, W. Liang, K. Wang, Z. Liu, J. Ma, and Q. Jin, “Spatial-temporal federated transfer learning with multi-sensor data fusion for cooperative positioning,” *Information Fusion*, vol. 105, p. 102182, 2024.

[9] X. Zhou, Q. Yang, X. Zheng, W. Liang, I. Kevin, K. Wang, J. Ma, Y. Pan, and Q. Jin, “Personalized federation learning with model-contrastive learning for multi-modal user modeling in human-centric metaverse,” *IEEE Journal on Selected Areas in Communications*, 2024.

[10] X. Zhou, X. Zheng, X. Cui, J. Shi, W. Liang, Z. Yan, L. T. Yang, S. Shimizu, I. Kevin, and K. Wang, “Digital twin enhanced federated reinforcement learning with lightweight knowledge distillation in mobile networks,” *IEEE Journal on Selected Areas in Communications*, 2023.

[11] X. Zhou, H. Huang, R. He, Z. Wang, J. Hu, and T. Tan, “Msra-sr: Image super-resolution transformer with multi-scale shared representation acquisition,” in *Proceedings of the IEEE/CVF International Conference on Computer Vision*, 2023, pp. 12 665–12 676.

[12] A. Amanatiadis, L. Bampis, and A. Gasteratos, “Accelerating single-image super-resolution polynomial regression in mobile devices,” *IEEE Transactions on Consumer Electronics*, vol. 61, no. 1, pp. 63–71, 2015.

[13] K. Wang, X. Yang, and G. Jeon, “Hybrid attention feature refinement network for lightweight image super-resolution in metaverse immersive display,” *IEEE Transactions on Consumer Electronics*, 2023.

[14] K. Jiang, Z. Wang, P. Yi, and J. Jiang, “Hierarchical dense recursive network for image super-resolution,” *Pattern Recognition*, vol. 107, p. 107475, 2020.

[15] C. Dong, C. C. Loy, K. He, and X. Tang, “Image super-resolution using deep convolutional networks,” *IEEE transactions on pattern analysis and machine intelligence*, vol. 38, no. 2, pp. 295–307, 2015.

[16] J. Kim, J. K. Lee, and K. M. Lee, “Accurate image super-resolution using very deep convolutional networks,” in *Proceedings of the IEEE conference on computer vision and pattern recognition*, 2016, pp. 1646–1654.

[17] J. Kim, J. K. Lee, and K. M. Lee, “Deeply-recursive convolutional network for image super-resolution,” in *Proceedings of the IEEE conference on computer vision and pattern recognition*, 2016, pp. 1637–1645.

[18] Y. Tai, J. Yang, and X. Liu, “Image super-resolution via deep recursive residual network,” in *Proceedings of the IEEE conference on computer vision and pattern recognition*, 2017, pp. 3147–3155.

[19] V. Dumoulin and F. Visin, “A guide to convolution arithmetic for deep learning (2016),” *arXiv preprint arXiv:1603.07285*, 2016.

[20] W. Shi, J. Caballero, F. Huszár, J. Totz, A. P. Aitken, R. Bishop, D. Rueckert, and Z. Wang, “Real-time single image and video super-resolution using an efficient sub-pixel convolutional neural network,” in *Proceedings of the IEEE conference on computer vision and pattern recognition*, 2016, pp. 1874–1883.

[21] C. Dong, C. C. Loy, and X. Tang, “Accelerating the super-resolution convolutional neural network,” in *Computer Vision–ECCV 2016: 14th European Conference, Amsterdam, The Netherlands, October 11–14, 2016, Proceedings, Part II 14*. Springer, 2016, pp. 391–407.

[22] B. Lim, S. Son, H. Kim, S. Nah, and K. Mu Lee, “Enhanced deep residual networks for single image super-resolution,” in *Proceedings of the IEEE conference on computer vision and pattern recognition workshops*, 2017, pp. 136–144.

[23] C. Tian, X. Zhang, J. C.-W. Lin, W. Zuo, Y. Zhang, and C.-W. Lin, “Generative adversarial networks for image super-resolution: A survey,” *arXiv preprint arXiv:2204.13620*, 2022.

[24] F. Yu, X. Wang, M. Cao, G. Li, Y. Shan, and C. Dong, “Osrt: Omnidirectional image super-resolution with distortion-aware transformer,” in *Proceedings of the IEEE/CVF Conference on Computer Vision and Pattern Recognition*, 2023, pp. 13 283–13 292.

[25] Y. Tai, J. Yang, X. Liu, and C. Xu, “Memnet: A persistent memory network for image restoration,” in *Proceedings of the IEEE international conference on computer vision*, 2017, pp. 4539–4547.

[26] N. Ahn, B. Kang, and K.-A. Sohn, “Fast, accurate, and lightweight super-resolution with cascading residual network,” in *Proceedings of the European conference on computer vision (ECCV)*, 2018, pp. 252–268.

[27] C. Tian, Y. Zhang, W. Zuo, C.-W. Lin, D. Zhang, and Y. Yuan, “A heterogeneous group cnn for image super-resolution,” *IEEE transactions on neural networks and learning systems*, 2022.

[28] Y. Zhang, Y. Tian, Y. Kong, B. Zhong, and Y. Fu, “Residual dense network for image super-resolution,” in *Proceedings of the IEEE conference on computer vision and pattern recognition*, 2018, pp. 2472–2481.

[29] Y. Chen, X. Dai, M. Liu, D. Chen, L. Yuan, and Z. Liu, “Dynamic convolution: Attention over convolution kernels,” in *Proceedings of the IEEE/CVF conference on computer vision and pattern recognition*, 2020, pp. 11 030–11 039.

[30] S. Wan, C. Gong, P. Zhong, B. Du, L. Zhang, and J. Yang, “Multiscale dynamic graph convolutional network for hyperspectral image classification,” *IEEE Transactions on Geoscience and Remote Sensing*, vol. 58, no. 5, pp. 3162–3177, 2019.

[31] Y. Ding, J. Feng, Y. Chong, S. Pan, and X. Sun, “Adaptive sampling toward a dynamic graph convolutional network for hyperspectral image classification,” *IEEE Transactions on Geoscience and Remote Sensing*, vol. 60, pp. 1–17, 2021.

[32] Z. Duan, T. Zhang, X. Luo, and J. Tan, “Dckn: multi-focus image fusion via dynamic convolutional kernel network,” *Signal Processing*, vol. 189, p. 108282, 2021.

[33] C. Dai, Z. Guan, and M. Lin, “Single low-light image enhancer using taylor expansion and fully dynamic convolution,” *Signal Processing*, vol. 189, p. 108280, 2021.

[34] J. Hou, Z. Guo, Y. Wu, W. Diao, and T. Xu, “Bsnet: Dynamic hybrid gradient convolution based boundary-sensitive network for remote sensing image segmentation,” *IEEE Transactions on Geoscience and Remote Sensing*, vol. 60, pp. 1–22, 2022.

[35] H. Shen, Z.-Q. Zhao, and W. Zhang, “Adaptive dynamic filtering network for image denoising,” in *Proceedings of the AAAI Conference on Artificial Intelligence*, vol. 37, no. 2, 2023, pp. 2227–2235.

[36] Z. Hui, X. Wang, and X. Gao, “Fast and accurate single image super-resolution via information distillation network,” in *Proceedings of the IEEE conference on computer vision and pattern recognition*, 2018, pp. 723–731.

[37] D. P. Kingma and J. Ba, “Adam: A method for stochastic optimization,” *arXiv preprint arXiv:1412.6980*, 2014.

[38] F. Yu and V. Koltun, “Multi-scale context aggregation by dilated convolutions,” *arXiv preprint arXiv:1511.07122*, 2015.

[39] A. Krizhevsky, I. Sutskever, and G. E. Hinton, “Imagenet classification with deep convolutional neural networks,” *Advances in neural information processing systems*, vol. 25, 2012.

[40] E. Agustsson and R. Timofte, “Ntire 2017 challenge on single image super-resolution: Dataset and study,” in *Proceedings of the IEEE conference on computer vision and pattern recognition workshops*, 2017, pp. 126–135.

[41] M. Bevilacqua, A. Roumy, C. Guillemot, and M. L. Alberi-Morel, “Low-complexity single-image super-resolution based on nonnegative neighbor embedding,” 2012.

[42] R. Zeyde, M. Elad, and M. Protter, “On single image scale-up using sparse-representations,” in *Curves and Surfaces: 7th International Conference, Avignon, France, June 24–30, 2010, Revised Selected Papers 7*. Springer, 2012, pp. 711–730.

[43] D. Martin, C. Fowlkes, D. Tal, and J. Malik, “A database of human segmented natural images and its application to evaluating segmentation algorithms and measuring ecological statistics,” in *Proceedings Eighth IEEE International Conference on Computer Vision. ICCV 2001*, vol. 2. IEEE, 2001, pp. 416–423.

[44] J.-B. Huang, A. Singh, and N. Ahuja, “Single image super-resolution from transformed self-exemplars,” in *Proceedings of the IEEE conference on computer vision and pattern recognition*, 2015, pp. 5197–5206.

[45] Y.-S. Xu, S.-Y. R. Tseng, Y. Tseng, H.-K. Kuo, and Y.-M. Tsai, “Unified dynamic convolutional network for super-resolution with variational degradations,” in *Proceedings of the IEEE/CVF Conference on Computer Vision and Pattern Recognition*, 2020, pp. 12 496–12 505.

[46] K. Simonyan and A. Zisserman, “Very deep convolutional networks for large-scale image recognition,” *arXiv preprint arXiv:1409.1556*, 2014.

[47] A. Hore and D. Ziou, “Image quality metrics: Psnr vs. ssim,” in *2010 20th international conference on pattern recognition*. IEEE, 2010, pp. 2366–2369.

[48] K. Jiang, Z. Wang, P. Yi, T. Lu, J. Jiang, and Z. Xiong, “Dual-path deep fusion network for face image hallucination,” *IEEE Transactions on Neural Networks and Learning Systems*, vol. 33, no. 1, pp. 378–391, 2020.

[49] R. Timofte, V. De Smet, and L. Van Gool, “A+: Adjusted anchored neighborhood regression for fast super-resolution,” in *Computer Vision–ACCV 2014: 12th Asian Conference on Computer Vision, Singapore, Singapore, November 1–5, 2014, Revised Selected Papers, Part IV 12*. Springer, 2015, pp. 111–126.

[50] D. Dai, R. Timofte, and L. Van Gool, “Jointly optimized regressors for image super-resolution,” in *Computer Graphics Forum*, vol. 34, no. 2. Wiley Online Library, 2015, pp. 95–104.

- [51] S. Schulter, C. Leistner, and H. Bischof, “Fast and accurate image upscaling with super-resolution forests,” in *Proceedings of the IEEE conference on computer vision and pattern recognition*, 2015, pp. 3791–3799.
- [52] Z. Wang, D. Liu, J. Yang, W. Han, and T. Huang, “Deep networks for image super-resolution with sparse prior,” in *Proceedings of the IEEE international conference on computer vision*, 2015, pp. 370–378.
- [53] X. Mao, C. Shen, and Y.-B. Yang, “Image restoration using very deep convolutional encoder-decoder networks with symmetric skip connections,” *Advances in neural information processing systems*, vol. 29, 2016.
- [54] K. Zhang, X. Gao, D. Tao, and X. Li, “Single image super-resolution with non-local means and steering kernel regression,” *IEEE Transactions on Image Processing*, vol. 21, no. 11, pp. 4544–4556, 2012.
- [55] Y. Chen and T. Pock, “Trainable nonlinear reaction diffusion: A flexible framework for fast and effective image restoration,” *IEEE transactions on pattern analysis and machine intelligence*, vol. 39, no. 6, pp. 1256–1272, 2016.
- [56] Z. Lu, Z. Yu, P. Yali, L. Shigang, W. Xiaojun, L. Gang, and R. Yuan, “Fast single image super-resolution via dilated residual networks,” *IEEE Access*, vol. 7, pp. 109 729–109 738, 2018.
- [57] Y. Shi, K. Wang, C. Chen, L. Xu, and L. Lin, “Structure-preserving image super-resolution via contextualized multitask learning,” *IEEE transactions on multimedia*, vol. 19, no. 12, pp. 2804–2815, 2017.
- [58] W.-S. Lai, J.-B. Huang, N. Ahuja, and M.-H. Yang, “Deep laplacian pyramid networks for fast and accurate super-resolution,” in *Proceedings of the IEEE conference on computer vision and pattern recognition*, 2017, pp. 624–632.
- [59] F. Cao and B. Chen, “New architecture of deep recursive convolution networks for super-resolution,” *Knowledge-Based Systems*, vol. 178, pp. 98–110, 2019.
- [60] C. Tian, R. Zhuge, Z. Wu, Y. Xu, W. Zuo, C. Chen, and C.-W. Lin, “Lightweight image super-resolution with enhanced cnn,” *Knowledge-Based Systems*, vol. 205, p. 106235, 2020.
- [61] J. Yang, J. Wright, T. S. Huang, and Y. Ma, “Image super-resolution via sparse representation,” *IEEE transactions on image processing*, vol. 19, no. 11, pp. 2861–2873, 2010.
- [62] J. Song, J. Xiao, C. Tian, Y. Hu, L. You, and S. Zhang, “A dual cnn for image super-resolution,” *Electronics*, vol. 11, no. 5, p. 757, 2022.
- [63] Y. Huang, S. Li, L. Wang, T. Tan *et al.*, “Unfolding the alternating optimization for blind super resolution,” *Advances in Neural Information Processing Systems*, vol. 33, pp. 5632–5643, 2020.
- [64] W. Shi, F. Tao, and Y. Wen, “Structure-aware deep networks and pixel-level generative adversarial training for single image super-resolution,” *IEEE Transactions on Instrumentation and Measurement*, vol. 72, pp. 1–14, 2023.
- [65] W. Bae, J. Yoo, and J. Chul Ye, “Beyond deep residual learning for image restoration: Persistent homology-guided manifold simplification,” in *Proceedings of the IEEE conference on computer vision and pattern recognition workshops*, 2017, pp. 145–153.
- [66] J. Xu, M. Li, J. Fan, X. Zhao, and Z. Chang, “Self-learning super-resolution using convolutional principal component analysis and random matching,” *IEEE Transactions on Multimedia*, vol. 21, no. 5, pp. 1108–1121, 2018.
- [67] J. Sahambi *et al.*, “A lightweight deep residual attention network for single image super resolution,” in *2023 National Conference on Communications (NCC)*. IEEE, 2023, pp. 1–6.
- [68] C. Tian, Y. Xu, W. Zuo, C.-W. Lin, and D. Zhang, “Asymmetric cnn for image superresolution,” *IEEE Transactions on Systems, Man, and Cybernetics: Systems*, vol. 52, no. 6, pp. 3718–3730, 2021.
- [69] Z. Luo, H. Huang, L. Yu, Y. Li, H. Fan, and S. Liu, “Deep constrained least squares for blind image super-resolution,” in *Proceedings of the IEEE/CVF Conference on Computer Vision and Pattern Recognition*, 2022, pp. 17 642–17 652.